Articles

Rheology of Cetyltrimethylammonium *p*-Toluenesulfonate−Water System. 3. Nonlinear Viscoelasticity

J. F. A. Soltero, F. Bautista, and J. E. Puig*

Departamento de Ingeniería Química, Universidad de Guadalajara, Boul. M. García Barragán # 1451, Guadalajara, Jal. 44430, Mexico

O. Manero

Instituto de Investigaciones en Materiales, Universidad Nacional Autónoma de México, Apdo. Postal 70-360, Mexico, D.F. 04510, Mexico

Received December 1, 1997

The nonlinear viscoelastic behavior of the cetyltrimethylammonium *p*-toluenesulfonate (CTAT)−water system is investigated in steady and unsteady shear flow as a function of surfactant concentration and temperature. A rheo-optical study which includes measurements of dichroism, birefringence, and turbidity under flow at various shear rates is also discussed. The shear viscosity data in steady shear agree with the complex viscosity in the limit of low deformation rates. For moderate deformation rates, in the shear thinning region, the Cox-Merz rule is not followed. In all cases, a limiting stress or plateau stress was observed at shear rates that exceed one-half of the reciprocal of the main relaxation time $[(2\tau_d)^{-1}]$. At the stress plateau, the micellar solution most likely undergoes an isotropic-to-nematic phase transition induced by shear. However, our results do not conclusively exclude the possibility of a constitutive instability with respect to shear banding, in which simultaneous shear rates coexist under controlled stress experiments. In unsteady shear flow, CTAT−water micellar solutions exhibit a slow transient behavior in which the system achieves steady state in starting up experiments after tens to hundreds of Maxwell relaxation times. This is consistent with the existence of shear banding. Metastable branches are also observed in thixotropic loops produced under exponential shear. The time scale of this branch coincides with that of the inception of shear flow just before the overshoot peak. Moreover, the system exhibits a quasilinear rheological behavior at long times characterized by an exponential relaxation with a single time constant. A simple model consisting of the co-deformational Maxwell constitutive equation and a kinetic equation for construction and destruction of structure is proposed to predict distinct features of the complex rheological behavior of the elongated micellar solutions.

Introduction

Cationic surfactants complexed with certain organic salts or acids often form threadlike micelles in aqueous solutions which exhibit intriguing viscoelastic behavior even in the dilute regime.[1−6] For instance, micellar solutions of cetyltrimethylammonium bromide (CTAB)−salicylic acid present two main relaxation mechanisms that may merge into a single one depending on the relative concentrations of the constituents.[7]

In concentrated polymer solutions, relaxation is governed by reptation of the macromolecules along their own contour through the entanglement network with a mesh size that depends on polymer concentration.[8] In a similar fashion, relaxation in an entangled micellar solution is partly due to reptation of the wormlike micelles.[9] However, in contrast to macromolecules, micelles can break and re-form continuously under the influence of flow and then the relaxation can also occur by breakdown of the entanglement network, presumably by segments passing through each other at the entanglement points.[5,9−12] In fact, the reptation−reaction theory developed by Cates indicates that when the average lifetime of the micelles is of the order of magnitude of the stress relaxation time, relaxation decays exponentially with a single time constant; i.e., a Maxwell behavior is observed.[9]

The same model, extended to the nonlinear rheology of wormlike micellar systems, predicts a saturation in the shear stress in steady shear measurements.[13,14] This behavior, observed experimentally in many micellar systems, is accompanied by slow transients, overshoots,

* To whom correspondence should be addressed.

(1) Gravshold, S. J. *J. Colloid Inrterface Sci.* **1976**, *57*, 575.
(2) Rehage, H.; Hoffmann, H. *Rheol. Acta* **1982**, *21*, 561.
(3) Shikata, T.; Sakaiguchi, Y.; Urakami, H., Tamura, A.; Hirata, H. *J. Colloid Interface Sci.* **1987**, *119*, 291.
(4) Shikata, T.; Hirata, H.; Kotaka, T. *Langmuir* **1987**, *3*, 1081.
(5) Shikata, T.; Hirata, H.; Kotaka, T. *Langmuir* **1988**, *4*, 354.
(6) Shikata, T.; Hirata, H.; Takatory, A.; Osaki, K. *J. Non-Newtonian Fluid Mech.* **1988**, *28*, 171.
(7) Shikata, H.; Hirata, H. *Langmuir* **1989**, *5*, 348.
(8) Doi, M.; Edwards, S. F. *Theory of Polymer Dynamics*; Oxford University Press: Oxford, 1986.
(9) Cates, M. E.; Candau, S. J. *J. Phys.: Condens. Matter* **1990**, *2*, 6869 and references therein.
(10) Cates, M. E. *Europhys. Lett.* **1987**, *4*, 497.
(11) Cates, M. E. *Macromolecules* **1987**, *20*, 2289.
(12) Cates, M. E. *J. Phys. (Paris)* **1988**, *49*, 1593.

10.1021/la971299a CCC: $18.00
Published on Web 02/09/1999

and normal stresses upon inception of flow.[15−20] The plateau where the stress becomes independent of shear rate has been interpreted as a purely mechanical instability where shear banding occurs.[13,14,16,17] However, others have proposed a first-order isotropic-to-nematic phase transition to explain the stress plateau.[18−20]

Nonlinear behavior in surfactant-based systems is detected when the applied shear rates are moderately high. Departures from the linear behavior with a single relaxation time have been observed in stress relaxation experiments, and they occur when the applied shear rate exceeds the reciprocal of the main relaxation time of the sample (τ_d^{-1}).[15] The reptation−reaction model, on the other hand, predicts that nonlinear behavior occurs at shear rates of the order of $2.6\tau_d^{-1}$.[13,14]

In the nonlinear viscoelastic regime, structural changes in steady shear flow lead to lower viscosities than those observed in linear oscillatory shear experiments, i.e., the Cox−Merz rule is not followed.[18,20−22] Stress relaxation experiments in these systems show a complicated behavior in the semidilute regime, where the network begins to deform. Under these conditions, Raushcher et al.[23] found that the reptation mechanism dominates the dynamic processes of relaxation with a stretched exponential decay and that the viscoelastic properties of these solutions are very similar to those of entangled polymer solutions.

Elsewhere we reported the linear rheological behavior of the cetyltrimethylammonium *p*-toluenesulfonate (CTAT)−water system from low to relatively high concentrations and found that the characteristic time scale of the breakage and re-formation of the threadlike micelles is shorter than that corresponding to the reptation process and that the micellar solutions behave almost as a Maxwell fluid—although deviations are observed at high frequencies or small times.[24,25] It is the aim of the present paper to examine the nonlinear rheological behavior of the CTAT−water system over a wide range of shear rates. Rheological measurements are complemented with a rheo-optical study that includes measurements of dichroism, birefringence, and turbidity under step-changes in shear rate and flow reversal. Experiments in simple shear and in transient flows are analyzed and compared with theoretical predictions of the Cates model and of a simple model consisting of the co-deformational Maxwell constitutive equation and a kinetic equation for construction and destruction of structure.[26] For simple shear flow, the equations of the model adopt the following forms:

$$\sigma + \frac{1}{G_0\varphi}\frac{d\sigma}{dt} = \frac{\dot\gamma}{\varphi} \quad (1)$$

$$\frac{d\varphi}{dt} = \frac{\varphi_0 - \varphi}{\lambda} + k(\varphi_\infty - \varphi)\sigma\dot\gamma \quad (2)$$

Here σ is the shear stress, $\dot\gamma$ is the shear rate, $\varphi(\equiv\eta^{-1})$ is the fluidity or the reciprocal of the shear viscosity (η), G_0 is the shear modulus, φ_0 and φ_∞ are the fluidities at zero and very high-shear rates, λ is a structure relaxation time, and k can be interpreted as a kinetic constant for structure breakdown.

Experimental Section

Cetyltrimethylammonium *p*-toluenesulfonate or CTAT (98% pure from Sigma) was further purified by recrystallization from a chloroform−ethyl ether mixture (50:50 by volume). Doubly distilled and deionized water was used.

Samples were prepared by weighing appropriate amounts of CTAT and water in glass vials. These vials were placed in a water bath at 60 °C for a week where they were frequently shaken by hand to accelerate homogenization. Then samples were placed in a water bath for 3 days at the temperature of measurement. All samples were centrifuged to remove suspended air bubbles before being tested.

Rheological properties were measured with a Carri-Med CSL-500 controlled stress rheometer and cone-and-plate geometry. The cone angle was 0.035 rad and the diameter was 4.0 cm. Steady shear measurements were done in a Rheometrics dynamical spectrometer RDS-II and a cone-and-plate geometry, but with a cone angle of 0.1 rad and a plate diameter of 2.5 cm. To prevent changes in composition for water evaporation during measurements, a humidification chamber containing wetted sponges was placed around the cone-and-plate fixture. To maintain constant the temperature during measurements, the humidification chamber contains a coil to circulate a thermostated fluid.

The rheo-optical measurements were done in a Rheometrics optical analyzer in the laboratory of Professor J. Mewis at Louvain, Belgium. This instrument uses a polarization modulation technique to measure both optical anisotropies, which is described in detail elsewhere.[27]

Results

Steady Simple Shear Flow. Figure 1 shows σ as a function of $\dot\gamma$ for a 10 wt % CTAT sample measured in a shear rate-controlled rheometer ("shear-mode") and in a stress-controlled rheometer ("stress mode"). At low shear rates, σ increases linearly with $\dot\gamma$ up to a critical shear rate ($\dot\gamma_p$) or shear stress (σ_p), where the stress becomes independent of shear rate. In the linear region, which corresponds to the Newtonian regime characterized by a Newtonian viscosity or zero-shear rate viscosity (η_0), both types of rheometers give identical results. However, once the plateau region is reached, there are significant differences between both rheometers. In the shear-mode, the plateau appears when a critical shear rate ($\dot\gamma_p$) is reached. On increasing shear rate, there is a bump in the stress that falls on the plateau at higher shear rates. Here it is noteworthy that the data points in the plateau region correspond to the steady state values, which are reached after times on the order of tens to hundreds of Maxwell relaxation times (see Figure 6). The second critical shear rate which corresponds to the end of the plateau could not be reached in our measurements because of flow instability. In the stress mode, on the other hand, the shear rate increases rapidly in a very narrow region of applied stress and then it oscillates between low and high values, which presumably correspond to the shear rates at the beginning

(13) Spenley, N. A.; Cates, M. E.; McLeish, T. C. B. *Phys Rev Lett.* **1993**, *71*, 939.
(14) Spenley, N. A.; Yuan, X. F.; Cates, M. E. *J. Phys. II* **1996**, *7*, 1071.
(15) Rehage, H.; Hoffmann, H. *Molecular Phys.* **1991**, *74*, 933; *J. Phys. Chem.* **1988**, *92*, 4712.
(16) Grand, C.; Arrault, J.; Cates, M. E. *J. Phys. II* **1997**, *6*, 551.
(17) Callahan, P. T.; Cates, M. E.; Rofe, C. F.; Smelders, J. B. F. A. *J. Phys. II* **1996**, *6*, 375.
(18) Berret, L. F.; Roux, D. C.; Porte, G. *J. Phys. II* **1994**, *4*, 1261.
(19) Berret, L. F. *Langmuir* **1997**, *13*, 2227.
(20) Decrupe, J. P.; Capelare, E.; Cressely, R. *J. Phys. II* **1997**, *7*, 257.
(21) Robles-Vásquez, O.; Corona-Galván, S.; Soltero, J. F. A.; Puig, J. E.; Tripodi, S. B.; Vallés, E.; Manero, O. *J. Colloid Interface Sci.* **1993**, *160*, 65.
(22) Soltero, J. F. A.; Robles-Vásquez, O.; Puig, J. E.; Manero, O. *J. Rheol.* **1995**, *39*, 1.
(23) Rauscher, A.; Rehage, H.; Hoffmann, H. *Prog. Colloid Polym. Sci.* **1991**, *84*, 99.
(24) Soltero, J. F. A.; Puig, J. E.; Manero, O.; Schulz, P. C. *Langmuir* **1995**, *11*, 3337.
(25) Soltero, J. F. A.; Puig, J. E.; Manero, O. *Langmuir* **1996**, *12*, 2654.
(26) Bautista, F.; De Santos, J.; Puig, J. E.; Manero, O. *J. Non-Newtonian Fluid Mech.* **1999**, *80*, 93.
(27) Yanase, H.; Moldenaers, P.; Mewis, J.; Abetz, V.; Van Egmond, J.; Fuller, G. G. *Rheol. Acta* **1991**, *30*, 89.

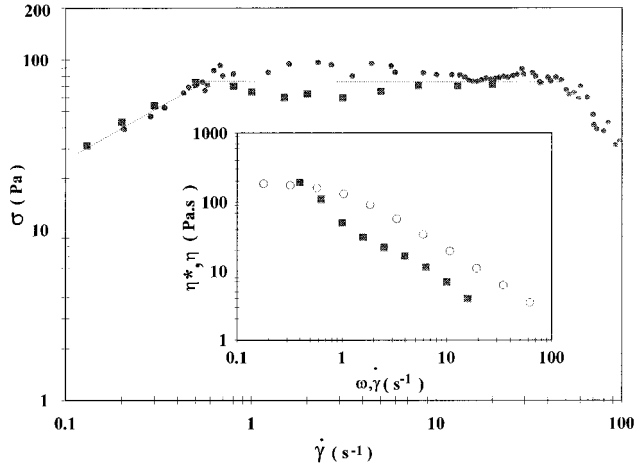

Figure 1. Shear stress (σ) as a function of shear rate ($\dot{\gamma}$) for 10 wt % samples measured at 30 °C in a controlled-strain rheometer (■) and in a controlled-stress rheometer (●). Dashed line is an aid to the eye. Inset: Shear viscosity (η) as a function of shear rate (■) and complex viscosity (η^*) as function of frequency (ω) (○) measured in a strain-controlled rheometer.

Table 1. Stress Relaxation Time (τ), Disentanglement Time ($\tau_d = 1/\omega_{CO}$), Elastic Plateau Modulus (G_0), Normalized Stress Plateau σ_p/G_0, and Weisenberg Number ($\dot{\gamma}_p\tau_d$) as a Function of CTAT Concentration Measured at 30 °C

C_{CTAT} (wt %)	stress relaxation		oscillatory measurements			
	τ (s)	G_0 (Pa)	τ_d (s)	G_0 (Pa)	σ_p/G_0	$\dot{\gamma}_p\tau_d$
3	5.4	19.5	5.3	19	1.2	3.9
5	2.3	43	2.4	41.5	0.98	1.8
10	0.91	164	0.97	176	0.47	0.34
15	0.56	390	0.51	380	0.37	0.25
20	0.42	640	0.32	620	0.34	0.20

and at the end of the plateau. In fact, we have observed the acceleration and deacceleration of the cone and plate of the constant-stress rheometer in the plateau region. When the stress is increased more rapidly, a metastable branch appears (see Figure 8) similar to that reported by Grand et al.[16]

The shear viscosity (η) as a function of $\dot{\gamma}$ and the complex viscosity ($\eta^* \equiv G^*/\omega$) as a function of frequency are shown in the inset of Figure 1. Both shear and complex viscosities are constant and equal to η_0 at low deformation rates (up to ca. 0.5 s^{-1}, which is about one-half of the reciprocal of the main relaxation time of this sample—Table 1). At larger shear rates, a shear thinning region is observed, where the shear viscosity follows a power law with a slope close to −1, in agreement with the existence of a limiting stress, i.e., σ_p. Complex viscosity also follows a power law with frequency with a slope of −1. In this region, however, η and η^* do not coincide; i.e., the Cox−Merz rule[28] is not followed. At shear rates of ca. 50 s^{-1}, the viscosity drops indicating a rapid fall of the stress with shear rate. It is noteworthy that for shear rates larger than 50 s^{-1}, the 10 wt % sample takes a gellike consistency and tends to slip on the surfaces of the cone−plate fixture. This observation is consistent with the appearance of turbidity and change in texture seen after the sample has been sheared. These results strongly suggest a shear-induced phase transition. Similar results were observed with samples at other concentrations.

Figure 2 shows σ versus $\dot{\gamma}$, measured in the shear mode,

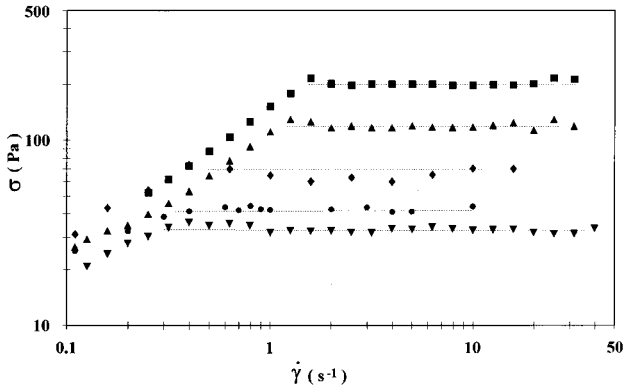

Figure 2. Shear stress (σ) versus shear rate ($\dot{\gamma}$) measured at 30 °C as a function of CTAT concentration: 3 (▼); 5 (●); 10 (◆); 15 (▲); 20 wt % (■). Dashed lines are aids to the eye.

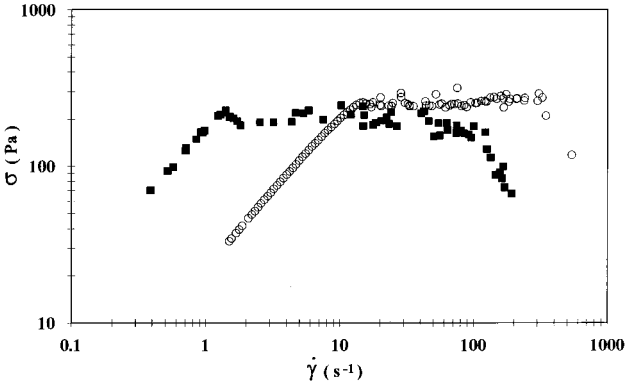

Figure 3. Shear stress (σ) as a function of shear rate ($\dot{\gamma}$) measured at 30 °C (■) and 40 °C (○) for 20 wt % CTAT samples.

as a function of concentration. All samples follow a straight line with slope of 1 up to a critical shear rate ($\dot{\gamma}_p$) where the stress plateau appears. Both $\dot{\gamma}_p$ and σ_p shift to larger values as the CTAT concentration is increased. Note also that the transition from the Newtonian regime to the stress plateau becomes sharper as the CTAT concentration is increased. Similar results have been reported elsewhere.[18]

Shear stress as a function of shear rate measured at 30 and 40 °C are shown in Figure 3 for a 20 wt % CTAT sample. Increasing the temperature shifts the critical shear rate ($\dot{\gamma}_p$) to higher values as a consequence of the Arrhenius-type dependence of the main relaxation time (τ_d) with temperature.[25] The shear-thinning region decreases almost 1 decade upon increasing temperature and the onset of instability, detected as a sharp drop in viscosity, shifts to higher shear rates as well.

Stress Relaxation upon Cessation of Steady Shear Flow. The normalized stress relaxation (σ/σ_{ss}) versus a dimensionless time (t/τ_d) as a function of shear rate after cessation of flow are shown in Figure 4 for a 10 wt % CTAT sample. For shear rates smaller than approximately 0.5 s^{-1} [$\approx(2\tau_d)^{-1}$], the stress relaxation is single exponential—note that the stress plateau in steady shear measurements also begins at $\dot{\gamma} \approx (2\tau_d)^{-1}$ (Figure 1). At the smallest shear rate examined (0.1 s^{-1}), the normalized stress relaxation coincides with data from step strain experiments.[29] For shear rates larger than 0.5 s^{-1}, the relaxation curves are no longer single exponential: they show fast decay, transition, and slow decay regions. The fast decay spans up to 0.2−0.5 s, depending on shear rate, whereas the slow decay extends to longer times. The slow- and the fast-relaxation times, obtained from the slopes of the

(28) Bird, R. B.; Armstrong, R. C.; Hassager, O. *Dynamics of Polymeric Liquids. Vol I*, **1987**.

(29) Soltero, J. F. A. Ph.D. Thesis, U.N.A.M., Mexico, 1995.

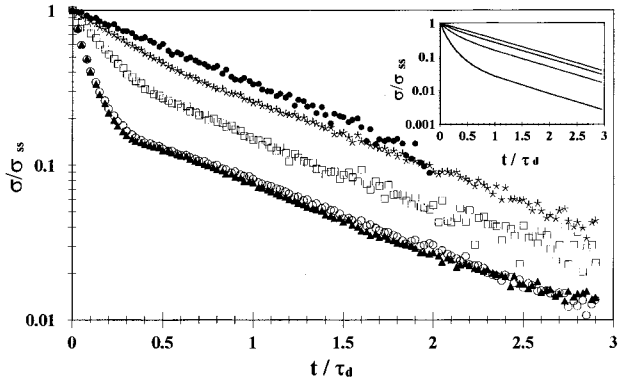

Figure 4. Normalized stress (σ/σ_{ss}) (where σ_{ss} is the steady-state shear stress) versus the normalized time (t/τ_d) as a function of shear rate after cessation of flow at 30 °C for 10 wt % CTAT samples: 0.1 (●); 0.5 (★); 1.0 (□); 5.0 (○); 10.0 s^{-1} (▲). Inset: Predictions of the model.

Table 2. Relaxation Time in the Fast (τ_1) and Slow Mode (τ_2) in Stress Relaxation after Cessation of Flow Experiments Performed at 30 °C as a Function of Shear Rate for a 10 wt % CTAT Solution[a]

$\dot{\gamma}$ (s^{-1})	τ_1 (s)	τ_2 (s)
0.1	0.89 (0.9091)	0.89 (0.9018)
0.5	0.88 (0.8977)	0.88 (0.9018)
1	0.77 (0.7670)	0.95 (0.9018)
5	0.13 (0.1988)	0.93 (0.9018)
10	0.13 (0.0956)	0.98 (0.9018)

[a] Numbers in parentheses represent the relaxation times predicted by our model.

relaxation decay curves, are reported in Table 2. Notice that the fast-relaxation time is sensitive to the value of the applied shear rate, i.e., it depends on the steady-state fluidity prior to relaxation, whereas the slow mode is monoexponential with a decay constant equal to the Maxwell relaxation time, τ_d [$\equiv(G_0\varphi_0)^{-1}$] (cf. Tables 1 and 2). Therefore, at long times one should expect lines with identical slopes whose ordinate is a function of the magnitude of ($\varphi_{ss} - \varphi_0$) (Figure 4).

Our model predicts a single-exponential decay when the applied shear rates are smaller than $(2\tau_d)^{-1}$ and a slow and a fast decays when the applied shear rates exceed this value (inset in Figure 4). The model mimics the slow and the fast stress decays for applied shear rates up to $(\tau_d)^{-1}$ (Table 2); for larger shear rates, it predicts stress decays faster than the experimental ones at short times, but it reproduces well the experimental limiting slope at long times (Table 2).

Inception of Shear Flow. Stress growth upon inception of shear flow versus t/τ_d as a function of shear rate are shown in Figure 5 for a 10 wt % CTAT sample. Maxwell behavior with a single time constant is detected at low shear rates. The increase of the stress with time can be reproduced with the Maxwell model and the value of τ_d of the sample. At higher shear rates, overshoots appear, which become bigger as the applied shear rate is increased. Note that the overshoots appear when the applied shear rate is approximately equal to $\dot{\gamma}_p$, i.e., around 0.5. s^{-1} [$\approx(2\tau_d)^{-1}$] (Figure 1). Also, for shear rates equal or larger than the critical value for the stress plateau ($\dot{\gamma}_p$), the time required to reach the steady state is several tens of the main relaxation time of the sample. Similar slow transients above $\dot{\gamma}_p$ have been reported elsewhere.[15,16] When plotted against strain (not shown), the first overshoot is located at about 1.4 strain units for shear rates around the reciprocal of the main relaxation time; the peak shifts to about 2.5 and 5 strain units when the shear rates are

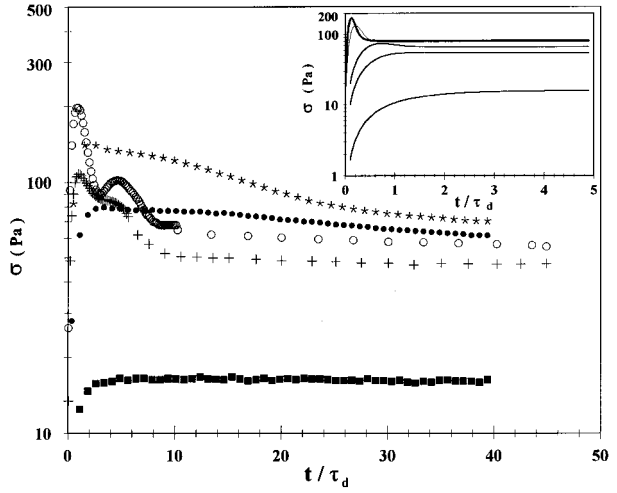

Figure 5. Stress growth (σ^+) upon inception of flow versus the normalized time (t/τ_d) at 30 °C as a function of applied shear rate for 10 wt % CTAT sample: 0.1 (■); 1.0 (●); 2.0 (+); 3.0 (★); 6.0 s^{-1} (○). Inset: Predictions of the model.

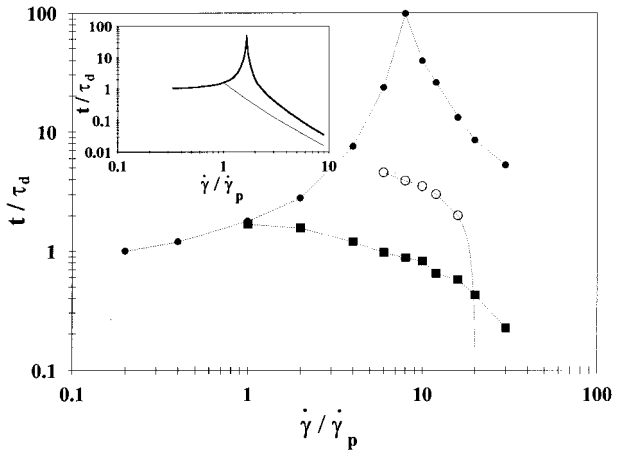

Figure 6. Normalized time (t/τ_d) versus normalized shear rate ($\dot{\gamma}/\dot{\gamma}_p$) at 30 °C for 10 wt % CTAT samples: steady state (●); first overshoot maximum (■); the second overshoot maximum (○). Inset: Predictions of the model.

5 and 10 s^{-1}, respectively. A characteristic feature is the appearance of stress oscillations at a shear rate of 2 s^{-1}. Also as the shear rate is increased, the period of the oscillations becomes larger until the oscillations disappear completely at shear rates around 10 s^{-1} (Figure 5).

To understand better the complex transient behavior of viscoelastic micellar solutions, in Figure 6 it is shown the time (in τ_d units) needed to reach the steady stress and those required for the first and the second overshoots to appear, as a function of the normalized shear rate ($\dot{\gamma}/\dot{\gamma}_p$). When the applied shear rate is smaller than the critical shear rate ($\dot{\gamma}/\dot{\gamma}_p < 1$), the steady-state value is reached in times of the order of the relaxation time of the sample; also, no overshoots are detected. However, as soon as $\dot{\gamma}$ exceeds $\dot{\gamma}_p$, the time needed to reach the steady-state value increases rapidly with increasing $\dot{\gamma}$, goes through a maximum, and then it decreases again as the second critical shear rate is reached, i.e., the shear rate at which the stress plateau ends. In our experiments, the second critical shear rate could not be reached because of flow instabilities (see Figures 1 and 3). Also, at $\dot{\gamma}/\dot{\gamma}_p = 1$, overshoots appear, whose magnitude increases with increasing applied shear rate; however, the position of the first overshoot shifts to smaller times upon increasing shear rates, until eventually, they disappear. A second

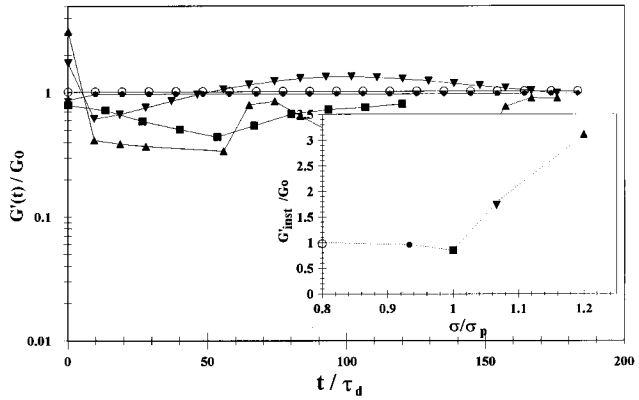

Figure 7. Normalized elastic modulus ($G'(t)/G_0$) versus normalized time (t/τ_d) for a 10 wt % sample at 90 rad/s and 20% strain immediatly after preshearing at different stresses: 60 Pa (○); 70 Pa (●); 75 Pa (■); 80 Pa (▼); 90 Pa (▲). Inset: Normalized instantaneous elastic modulus (G_{inst}'/G_0) versus normalized stress (σ/σ_p) at 60 (○); 70 (●); 75 (■); 80 (▼); 90 Pa (▲). G_0 is the plateau elastic modulus and σ_p is the stress in steady shear measurements.

overshoot is another feature detected in the transient experiments of viscoelastic micellar solutions.[16] The second overshoot first appears at several $\dot{\gamma}/\dot{\gamma}_p$ units and rapidly vanishes upon increasing shear rate. The time when the second overshoot appears also shifts to lower values as $\dot{\gamma}/\dot{\gamma}_p$ increases.

Our model, which has to be solved numerically for this situation, predicts a Maxwell behavior with a single relaxation time when the applied shear rate is small, overshoots that increase in magnitude with increasing shear rate once a critical shear rate is exceeded, and an overshoot followed by a single undershoot in an intermediate shear rate interval (inset in Figure 5). For larger shear rates, the model predicts that the oscillations disappear completely; however, it underestimates the magnitude of the stress overshoots and the amplitude of the oscillations. Inset of Figure 6 depicts the predicted time required to reach steady values and that at which the first overshoot appears. The comparison of the predictions with data in Figure 6 reveals that the main experimental features are reproduced by the model except for the second overshoot which is not predicted by our model. On the other hand, when the corotational Maxwell constitutive equation, which includes a term for vorticity,[28] is coupled to the kinetic equation (eq 2), the second overshoot appears.[30]

Presheared Dynamical Experiments. To obtain more information about the structure of the samples below and above the stress plateau, samples were presheared in a stress-controlled rheometer at a stress below, equal, or larger than σ_p and then they were immediately subjected to oscillatory measurements at a constant frequency of 10 s^{-1} and strain amplitudes within the linear viscoelastic region. Under this conditions, the elastic response is roughly equal to the plateau modulus, G_0.[25] Figure 7 shows $G'(t)/G_0$ as a function of t/τ_d for 10 wt % CTAT samples presheared at different stress values. When the applied stress is smaller than σ_p, the instantaneously measured elastic modulus (G_{inst}') is equal to G_0. However, when the preshearing stress exceeds σ_p, G_{inst}' becomes larger than G_0, and it takes more than $100\tau_d$ to reach the steady plateau modulus. For even larger stresses, $G'(t)$ oscillates, and for the larger preshearing stress ($\approx 1.35\sigma_p$), the oscillations last more than $200\tau_d$. Inset in Figure 7 depicts G_{inst}'/G_0 as a function of σ/σ_p where it is observed that G_{inst}'/G_0 grows rapidly with increasing σ/σ_p once the preshearing stress becomes larger than σ_p. This may be due to a shear-induced phase transition at the stress plateau region. Moreover, the increase in G_{inst}'/G_0 as the preshearing stress is increased beyond σ_p suggests that the proportion of the more structured phase is increasing.

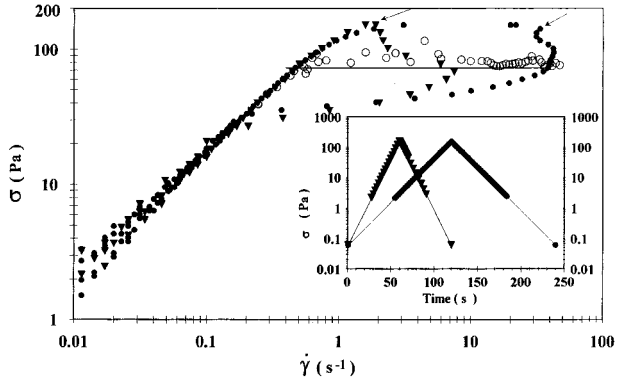

Figure 8. Thixotropic loops in increasing−decreasing shear stress cycle measured at 30 °C for a 10 wt % sample from 0.06 to 150 Pa for different cycle times: 120 s (▼); 240 s (●); steady-state data (○). The arrows represent the increasing−decreasing limit. Solid line is an aid to the eye. Inset: Program of the applied stress versus time.

Increasing−Decreasing Shear Stress Experiments. Controlled-stress experiments were performed in samples with concentrations between 3 and 20 wt % CTAT at various temperatures (30, 35, and 40 °C) and flow conditions. Here samples are subjected to increasing and decreasing shear stress cycles (in a logarithm mode) as a function of time to provide information on the microstructure modifications that occur in unsteady flow situations where the sample is not allowed to reach equilibrium conditions. A thixotropic sample will display a hysteresis loop in this type of cycles of strong shear flow.

In general, a thixotropic behavior is observed in these systems at high shear rates because the flow induces substantial microstructure modifications, which are preserved down to the low shear rate region. Figure 8 depicts typical results where the maximum stress was chosen to be larger than the critical stress ($\sigma_p \approx 81$ Pa) for this sample (10 wt % CTAT); for comparison, the steady-state response is included as a solid line in Figure 8. In these experiments, the maximum stress is maintained at 150 Pa but the duration of the entire cycle is varied (inset in Figure 8). When the applied stress is smaller than σ_p, i.e., within the Newtonian region, the steady state curve and the transient data coincide independently of the duration of the cycle. However, when the applied stress becomes equal to σ_p, the transient stresses exceed the plateau stress and yield a metastable branch. In this region, the shape of the branch (or upper loop) is strongly dependent on the duration of the cycle. When the cycle is performed faster (▼ in Figure 8), transient values go rapidly to the maximum applied stress and then fall below the plateau as the cycle is reversed. Notice that the transient stresses meet the Newtonian region at stress levels smaller than σ_p because there is not enough time for structure recovery. On the other hand, when the cycle is performed at a slower rate, the transient data (● in Figure 8) follow the *same* metastable branch as the faster cycle but then they jump to a much higher shear rate before falling below the steady plateau as the cycle is reversed; then transient data follow the same path as that in the fast cycle suggesting that the time between data points is much faster in both cycles

(30) Bautista, F., Ph.D. Thesis, Universidad de Guadalajara, Mexico, **1998**.

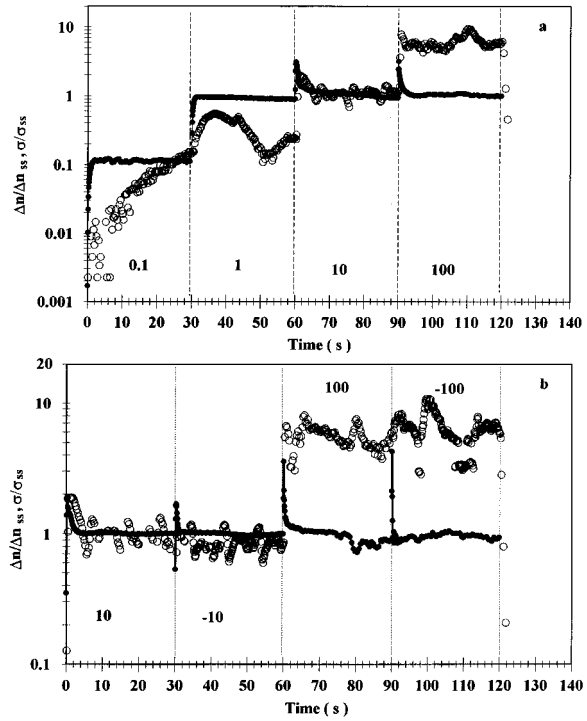

Figure 9. (a) Normalized stress (●) and birefringence (○) for a 5 wt % CTAT micellar solution subjected to step changes in shear rate. Normalization was done with values of the steady stress and birefringence at 10 s^{-1}. (b) Normalized stress (●) and birefringence (○) for a 5 wt % CTAT micellar solution subjected to flow reversal at 10 $^{-1}$ and at 100 s^{-1}. Normalization was done with values of the steady stress and birefringence at 10 s^{-1}.

than that required to reach steady-state conditions. Incidentally, for shear rates higher than 100 s^{-1}, a region of instability was observed, which is more apparent at higher CTAT concentrations. As mentioned before, the instability may be related to the shear-induced formation of a gellike phase (Figure 1). Evidently, the formation of the hysteresis loops appears to be a consequence of the slow transients in these systems and the formation of a different structure at stresses above σ_p.

Optical Measurements. A rheo-optical study as a function of shear rate, which includes measurements of dichroism, birefringence, and turbidity, was carried out on a 5 wt % CTAT solution. Flow birefringence measures the overall deformation and orientation of segments in the material and reflects an average over the polarizability of the micelles. In the measurements performed, birefringence turns out to be negative, which indicates a larger polarizability normal to the micellar axis than that parallel to such axis.[31] This polarizability arises from the fact that micelles are assemblies of surfactant chains oriented perpendicular to the micellar axis.

Figure 9a shows the stress and the birefringence against time for a 5 wt % CTAT solution at 30 °C as the shear rate is increased in a step fashion in decades from 0.1 to 100 s^{-1}. Magnitudes of the stress and of the birefringence are normalized with respect to their values at $\dot{\gamma} = 10$ s^{-1}. Birefringence and stress grow at different time scales upon inception of shear flow at $\dot{\gamma} = 0.1$ s^{-1}: birefringence grows monotonically in a time scale about 10 times longer than the stress—although both exhibit only a single characteristic time, i.e., both follow Maxwell behavior with different rate constants. As the shear rate exceeds the

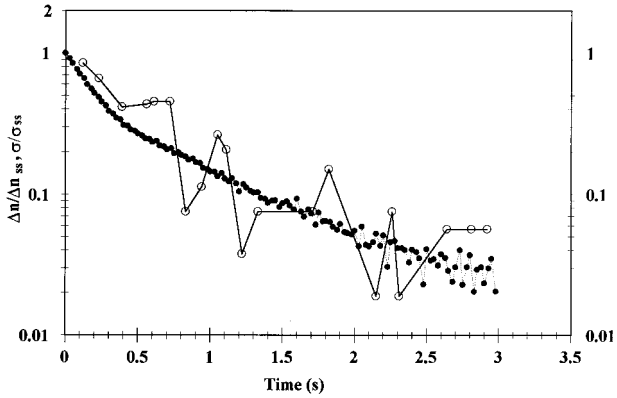

Figure 10. Normalized stress (●) and birefringence (○) relaxation after cessation of flow at $\dot{\gamma} = s^{-1}$.

reciprocal of the main relaxation time, which is 2.3 s for this sample (Table 1), the birefringence shows oscillations and the stress departs from the Maxwell behavior. This characteristic shear rate signals the onset of the plateau region of the shear stress for this sample.[29] At 10 s^{-1}, well within the plateau region of shear stress, a stress overshoot is observed at short times, followed by a small shoulder and a decay to steady values (Figure 9a). Simultaneously, an overshoot and oscillations with a regular period in the birefringence are detected. This overshoot is smaller than that of the stress and it appears at longer times. At the highest shear rate (100 s^{-1}), both the stress and the birefringence become unstable, displaying chaotic oscillations.

Shear stress and birefringence for a 5 wt % solution are shown in Figure 9b for consecutive forward-reversed flows at 10 and 100 s^{-1}. Again, stress and birefringence are normalized with respect to their values at 10 s^{-1}. At the inception of shear flow, both stress and birefringence display overshoots roughly of the same magnitude, but the birefringence peak appears at longer times. Upon flow reversal, the stress shows an overshoot of the same magnitude as that at the inception of shear flow. The maximum in the stress, as described elsewhere,[19] is related to a transition from a flow that is homogeneous shortly after the inception of shear but that becomes inhomogeneous as time evolves. The oscillations in the birefringence, on the other hand, are the result of the orientation of the micelles in an inhomogeneous flow (i.e., shear-banding), with periodic oriented−disoriented micellar structures.[32] Birefringence oscillates after the overshoot, and upon flow reversal, there is no overshoot, although the oscillations remain. In the parallel plate geometry, light propagates parallel to the direction of the velocity gradient and, therefore, optical anisotropies are measured in the plane defined by the flow direction and the vorticity axis. Upon flow reversal, the direction of these anisotropies does not change and remain in the same plane, producing similar birefringence oscillations.

Figure 10 depicts the normalized stress and birefringence relaxation upon cessation of flow for a 5 wt % CTAT sample at 30 °C. Birefringence fluctuations are observed, but both stress and birefringence relax approximately with the same time scale. Birefringence relaxation at several shear rates demonstrates that the anisotropic−isotropic transition takes place during the stress relaxation time scale. This is in contrast to the results given at the inception of flow (Figure 9a), where the stress and birefringence overshoots take place at different times,

(31) Wheeler, E. K.; Izu, P.; Fuller G. G. *Rheol. Acta* **1996**, *35*, 139.

(32) Cappelaere, E.; Cressely, R.; Decruppe, J. P. *Colloid Surfaces* **1995**, *104*, 353.

because within the time scale of the stress overshoot, the flow is still homogeneous but the birefringence captures the effects of banded flow.[14]

Dichroism is sensitive to structures of the order of the wavelength of light and, hence, it provides information on microstructure anisotropy. Dichroism for the 5 wt % CTAT micellar solution increases monotonically at the inception of shear flow for shear rates around the onset of the stress plateau region (1 s^{-1}) and it achieves steady state past 10 strain units (not shown). As shear rate increases, well within the plateau region, dichroism oscillates with periods that become shorter as the shear rate is increased. Upon cessation of flow, the oscillations are damped but the dichroism does not relax to zero like the birefringence. The extremely slow dichroism relaxation may be related to the presence of gellike structures formed at high shear rates. In fact, as described before, samples are turbid and exhibit different texture after been sheared because of the formation of aggregated structures, which are readily detected by the long relaxation dichroism. The time scale of this process is much longer than those of the stress and the birefringence, as the structural relaxation is determined by the diffusivities of the micelles forming the aggregates. Very long relaxation times in dichroism have also been observed in shear-thickening suspensions.[33]

Turbidity is related to dichroism and is proportional to the concentration and size of the micelles. Transmitted light intensity measurements demonstrate an increase in turbidity during step changes in shear rate, which become quite large as the shear rate is increased (not shown). After cessation of flow, the turbidity of the 5 wt % CTAT sample remains for several minutes.

Discussion

Similar to threadlike micellar systems that exhibit a fast breaking−re-forming regime ($\tau_{break}/\tau_{rep} \ll 1$),[16] the CTAT micellar solutions exhibit a stress plateau (Figures 1−3), slow transients (Figure 5), and metastability (Figure 8). Unstable flow in the CTAT/water system above a critical shear rate ($\dot{\gamma}_p$) or shear stress (σ_p) is indicated by the differences between results obtained with the stress-controlled rheometer and those yielded by the strain-controlled rheometer (Figure 1). The strain-controlled data show a bump within the stress plateau, whereas in the stress-controlled experiment a region of very fast increase of strain in a very narrow region of applied stress is detected.[17] Grand et al.[16] pointed out that the very slow relaxation processes occur near the metastable branch of the flow curve. This metastable branch is located above the true steady-state curve and it appears when the stress is increased relatively fast (fast enough not to reach steady-state conditions) under controlled stress conditions. The metastable branch also shows up in an increasing strain rate sweep at controlled strain rate, giving rise to a bump in the measured curve.

Explanations of such behavior have been given elsewhere.[13,14,17−19] Spenley et al.[13,14] consider that elongated micellar solutions exhibit a mechanical instability of shear banding type at a critical shear stress (σ_p), where bands of a highly sheared fluid of low viscosity coexist with a more viscous one supporting a lower shear rate. Alternatively, Berret et al.[18] and Berret[19] have proposed the coexistence of two thermodynamically stable phases (isotropic and nematic) within the sheared solution to account for the stress plateau. At low shear rates, the micellar solution is entirely isotropic in a truly homogeneous flow, which accounts for the initial linear stress−shear rate zone. At high shear rates, the flow is also homogeneous, but the sample is an oriented nematic phase. At intermediate shear rates, within the shear thinning region, the flow is nonhomogeneous (biphasic) and the shear rate acts on the relative proportions of each phase.

Strong evidence supporting the shear banding mechanism has been provided by NMR velocity imaging spectroscopy in a dilute cetylpyridinium chloride (CPCl)/sodium salicylate (60 mM//60 mM) solution. On the other hand, Berret et al.[35] presented a conclusive SANS study demonstrating a shear-induced first-order isotropic-to-nematic transition in the CPCl/hexanol/0.2 M NaCl brine. However, the micellar system that Berret et al. studied contains 31% surfactant concentration, and a nematic phase is nearby in the static phase diagram. Recently, on the other hand, Decruppe et al.[20] reported an optical and rheological study of semidiluted equimolar solutions of CTAB and KBr (0.3 M) and concluded that a nematic phase may be forming once the critical shear rate for the stress plateau is exceeded.

In the CTAT/water system, on the other hand, the mechanical instability of shear banding type which gives rise to the stress plateau, slow transients, and metastable branches, is detected from dilute (3% CTAT) to concentrated solutions (25%) (Figure 2). Although we have no strong experimental evidence to decide for any of the two proposed mechanism, some of our results suggest that a first-order phase transition is responsible for the formation of the stress plateau. The samples take a gellike consistency at high shear rates and exhibit an increase in turbidity during step changes in shear rate, which becomes quite large as the shear rate is increased; after cessation of flow, the turbidity of the sample remains for several minutes. The extremely slow dichroism relaxation also suggests the presence of gellike structures formed at high shear rates. The transition induced by shear toward an oriented nematic phase may account for the onset of flow instability observed as the shear rate is increased, i.e., the precipitous fall of shear stress at high shear rates (Figures 1 and 3). A concomitant oscillation in the optical properties, such as birefringence, is also observed within the region past the critical shear rate (Figure 9). The oscillations in the optical properties at shear rates corresponding to the stress plateau may be ascribed to a time-dependent oriented−disoriented micellar structures within a "banded flow" or nonhomogeneous biphasic flow, which becomes unstable at shear rates of the order of 100 s^{-1}.[19] Oscillations in the stress, on the other hand, a purely mechanical instability, are associated with the nonmonotonic stress−shear rate behavior. The magnitude of this shear rate (100 s^{-1}) is close to the value where the shear viscosity drops, which may be related to a shear-induced phase transition (Figure 1).

The nonobservation of the Cox−Merz rule (Figure 1) and the departure from linear behavior in stress relaxation experiments when the applied stress exceeds the critical shear rate (Figure 4), are also indicative of a phase transition.[36] In fact, for $\gamma > \dot{\gamma}_p$ the relaxation curve presents a slow relaxation time, which is shear rate independent, and a fast relaxation time, which depends on shear rate. The slow relaxation time is identical to the stress relaxation time of the micellar solution, whereas the fast relaxation time tends to a limiting value as the applied

(33) Haene, P. D.; Mewis, J.; Fuller, G. G. *J. Colloid Interface Sci.* **1991**, *156*, 150.

(34) Berret, J. F.; Roux, D. C.; Porte, G.; Lindner, P. *Europhys. Lett.* **1994**, *25*, 521.

(35) Ait-Ali, A.; Makhloudi, ER. *J. Rheol.* **1997**, *41*, 307.

(36) Fischer, P.; Rehage, H. *Rheol. Acta* **1997**, *36*, 13.

shear rate is increased (Figure 4). We propose that the slow relaxation time corresponds to the micellar solution whereas the fast relaxation one corresponds to the shear-induced nematic phase. Incidentally, the relaxation time of the 30 wt % CTAT hexagonal liquid crystalline sample ($\tau_d \approx 0.29$ s)[25] is similar to the limiting fast relaxation time (Table 2).

Preshearing-dynamical experiments also support the hypothesis of a phase transition induced by shear when the applied stress is larger than σ_p (Figure 7). When the preshearing stress is smaller than σ_p, the instantaneously measured elastic modulus (G_{inst}') is equal to G_0 indicating that no structural changes nor shear banding are occurring at these levels of stress. However, as soon as the preshearing stress surpasses σ_p, G_{inst}' becomes larger than G_0 and it takes tens to hundredths relaxation times to reach the steady plateau modulus, G_0. These results strongly suggested the formation of bands of an ordered (nematic) phase and of the micellar solution; also, that G_{inst}'/G_0 is increasing rapidly above unity as $\dot{\gamma}/\dot{\gamma}_p$ increases indicates that the proportion of the oriented phase is increasing. It is noteworthy that G_0 of the 30 wt % CTAT hexagonal sample is larger than those of the micellar solutions.[25] Moreover, these experiments demonstrate that the slow transients are related to the transition from homogeneous to inhomogeneous flow in the stress plateau region.

The effect of CTAT concentration (Figure 2) and of temperature (Figure 3) on the magnitudes of $\dot{\gamma}_p$ and σ_p can be readily explained in terms of the reaction−reptation theory. According to this theory, $\dot{\gamma}_p$ and σ_p are proportional to τ_d^{-1} and G_0, respectively,[13,14] where the values of the proportionality constants are model dependent.[16] For the CTAT/water micellar solutions, τ_d decreases whereas G_0 increases with increasing CTAT concentration (Table 1). Hence, one should expect that upon increasing the CTAT concentration, both $\dot{\gamma}_p$ and σ_p should shift to larger values (Figure 2). On the other hand, τ_d follows an Arrhenius behavior with temperature whereas G_0 is fairly independent of temperature—at least, in the temperature range examined.[25] Hence, σ_p should remain invariant to temperature changes whereas $\dot{\gamma}_p$ should shift to larger values as the temperature is increased (Figure 3).

The reaction−reptation theory predicts that σ_p/G_0 and the Weissenberg number, $\dot{\gamma}_p\tau_d$, are equal to 0.67 and 2.6, respectively.[13,14] However, serious discrepancies to these values, which presumably are model-dependent, have appeared in the literature.[19,35,36] Our results also disagree with the predictions of the reaction−reptation theory. In fact, σ_p/G_0 varies with CTAT concentration from 1.20 for the 3 wt % CTAT to 0.34 for the 20 wt % CTAT (Table 1). Moreover, we found that $\sigma_p/G_0 \propto [C_{CTAT}]^{-0.92}$. Also, $\dot{\gamma}_p\tau_d$ changes in a monotonic fashion with concentration from 3.9 for the 3 wt % CTAT sample to 0.20 for the 20 wt % sample (Table 1).

At this point it is noteworthy that the reaction−reptation theory predicts that the stress becomes independent of shear rate in the nonlinear viscoelastic region for micellar systems in the *fast breaking* regime.[13,14] This is not the case for the CTAT micellar solutions, where τ_{break}/τ_{rep} is of the order of 0.1 and deviations from Maxwell behavior with a single time constant are observed.[25] In fact, two relaxation processes in the CTAT micellar solutions have been detected in oscillatory measurements within the linear viscoelastic regime where the variation of the dynamic moduli with frequency is controlled by a single time constant (τ_d) in the low and intermediate frequency regions and by a second relaxation time in the high-frequency region.[25] The second relaxation process results in a linear dependence of the viscous modulus with frequency in the high-frequency region—this dependence is predicted by the Hess model at low concentrations and by the Doi−Edwards model at higher concentrations.[25] Therefore, the longest relaxation time, measured in oscillatory experiments, controls the dynamics in the low- and intermediate-frequency regions and the stress relaxation process at longer times. The time scale of the fast process in stress relaxation measurements is, however, quite different from that corresponding to the second relaxation process detected at high frequencies in oscillatory experiments. The time scale of the high-frequency oscillatory process is on the order of 0.01 s, which is 1 decade smaller than that of the fast stress relaxation process, which is around 0.1 s (Table 2).

Berret detected large deviations from the reaction−reptation model in the rheological data obtained at CPCl/NaCl at a concentration of 12% and found better agreement with the Johnson and Segalman phenomenological model.[19] In addition to the prediction of the nonmonotonic stress−shear rate curve at a critical stress, this model also predicts oscillations in inception of shear flow at shear rates above the plateau region. One important drawback of the Johnson and Segalman model is that it predicts periods of oscillations that are constant when expressed in terms of stress units, which is not what it is observed experimentally.

Fisher and Rehage[36] applied the Giesekus model to predict the flow of micellar systems in the nonlinear viscoelastic regime. These authors showed that the Giesekus model works in the concentration regime in which the reptation−reaction model fails. In fact, at specific salt/surfactant concentration ratio (C_{salt}/C_{surf}) in the CPCl/NaCl micellar system, there is a region of decreasing shear viscosity with increasing C_{salt}/C_{surf} such that the flow regime shows the instabilities reported for banded flow; outside this region, by increasing C_{salt}/C_{surf}, a much simpler rheological behavior is detected and the predictions of the reaction−reptation theory do not reproduce the experimental behavior. The Giesekus model predicts a stress plateau (without the high shear rate branch), the Cox−Merz rule, the Yamamoto relation, and both the Gleissle mirror relations when the anisotropy factor is 0.5.[36]

Here we introduce a very simple model that couples an upper-convected Maxwell constitutive equation with an evolution equation for the breaking and re-formation of the micelles (or any other aggregates) to predict the nonlinear rheological behavior of threadlike micellar systems.[26] From a phenomenological point view, the micellar breaking and re-formation processes, which lead to changes in the microstructure of the system, may be simulated with a model that combines the effect of flow and time on the instantaneous state of the microstructure. In fact, the time evolution of the fluidity (or inverse of viscosity) was derived taking into account the idea of changes in the network connectivity as a function of flow and time. In this sense, the model presented here contains the basic ingredients of a transient network model in which the phenomenological parameters may be related with real physical quantities if comparison with a microscopic theory or experiments are made. Furthermore, the idea of coupling an evolution equation for microstructural changes with the Maxwell constitutive equation is based on the idea that in the linear viscoelastic regime (i.e., small deformations and rates of deformation), the system behaves almost as a Maxwell fluid. Hence, by coupling a kinetic equation for re-formation and breaking of the micelles induced by flow to the Maxwell model, it is possible

Table 3. Values of the Parameters Used in the Model as a Function of CTAT Concentration

C_{CTAT} (wt %)	φ_0 (Pa•s)$^{-1}$	φ_∞ (Pa•s)$^{-1}$	$k \times 10^{-6}$ (Pa^{-1})	λ (s)	G_0 (Pa)
5	0.0275 ± 0.00005	19.8 ± 4	250.0 ± 20	0.12 ± .02	41.5 ± 5
10	0.0061 ± 0.00005	15.0 ± 3	30.3 ± 3	0.33 ± 0.05	176.0 ± 10
15	0.0050 ± 0.00005	12.6 ± 3	10.5 ± 1	0.38 ± 0.06	380.0 ± 25
20	0.0042 ± 0.00004	12.0 ± 3	4.2 ± 0.4	0.42 ± 0.06	620.0 ± 30

to reproduce quite well the steady shear data (Figures 1−3) and in particular the stress plateau. Moreover, our model predicts that the Cox-Merz rule *is not followed*, in agreement with experimental results (Figure 1). These features, incidentally, are *not* predicted by the corotational Maxwell model alone. Our model gives general expressions for the ratios τ_p/G_0 and $\dot{\gamma}_p/\tau_d$ as a function of the parameters of the model—these parameters can be obtained independently from rheological measurements.[26,30] In Table 3 are reported the values of the parameters of the model as a function of CTAT concentration. This property makes the model more flexible for predicting the experimental linear and nonlinear rheological behavior. Furthermore, our model predicts the very long relaxation times required to reach steady-state conditions (Figure 6), metastability and hysteresis (Figure 8), a relaxation function with two characteristic times when the applied stress exceeds $\dot{\gamma}_p$ and quasi linear behavior for shear rates smaller than $\dot{\gamma}_p$ (Figure 4), an overshoot, and an undershoot at the inception of shear flow experiments (Figure 5). Discrepancies between model and experiments, of course, are due in part to the linear form of the equation of the evolution of the structure (eq 2). For example, predictions shown in Figure 4 coincide with experiments at low shear rates but diverge at high shear rates. This limitation is also observed in Figure 5, where the magnitude of the predicted overshoot by the model is lower than that of the experiments. Similarly, the time to attain steady state in Figure 6 is underpredicted by the model. In both cases, the model underestimates the initial elastic response at the inception of flow, which is important in the prediction of oscillations. This limitation may be resolved by suggesting a more complicated nonlinear, time-dependent equation for the evolution of the structure, but the solution to the system of equations in most situations would be entirely numerical, losing their analytical simplicity. New approaches to this problem are being considered at present.

The model presented here is intended to predict nonlinear viscoelastic effects in systems where kinetic processes of breakage and re-formation take place simultaneously to changes in microstructure due to the flow. In this sense we think that the present model contains the relevant physics and the basic ingredients from a phenomenological point of view, as any other valid model. The extension of the present model to oscillatory measurements will be reported shortly.[30]

Acknowledgment. This work was supported by the Consejo Nacional de Ciencia y Tecnología de México (Grant No. 3397-E). Optical measurements were made at the laboratory of Professor Mewis in Louvain, Belgium, to whom we are indebted.

LA971299A